^{1}H NMR study of proton dynamics in $Cs_5H_3(SO_4)_4 \cdot xH_2O$

Koh-ichi Suzuki* and Shigenobu Hayashi†
Research Institute of Instrumentation Frontier, National Institute of Advanced Industrial Science and Technology (AIST), Tsukuba Central 5, 1-1-1 Higashi, Tsukuba, Ibaraki 305-8565, Japan
(Received 22 May 2006; revised manuscript received 3 July 2006; published 18 October 2006)

Complicated phase relations in $Cs_5H_3(SO_4)_4 \cdot xH_2O$ are revealed by thermal analyses. A superprotonic phase transition takes place at 420 K for both the hydrated and the anhydrous forms. The ^{1}H magic-angle-spinning (MAS) NMR spectra were traced at room temperature and at Larmor frequency of 400.13 MHz. The ^{1}H chemical shifts of the acidic protons are 10.9 and 11.2 ppm for the hydrated and the anhydrous forms, respectively. The hydrated sample shows a signal at 9.7 ppm additionally, which is ascribed to H_3O^+. Proton dynamics has been studied by ^{1}H static NMR spectra and spin-lattice relaxation times, T_1. In both a room-temperature phase (phase RT) and a high-temperature phase (phase HT), translational diffusion of protons takes place. The ^{1}H mean residence times in phase RT are obtained from the second moment analysis; $E_a = 49$ kJ mol^{-1} and $\tau_0 = 1.8 \times 10^{-11}$ s for the anhydrous form and $E_a = 31$ kJ mol^{-1} and $\tau_0 = 2.2 \times 10^{-9}$ s for the hydrated form. From the analysis of ^{1}H T_1 results we have obtained parameters of proton diffusion for phase HT; $E_a = 34$ kJ mol^{-1} and $\tau_0 = 3 \times 10^{-13}$ s for the anhydrous form and $E_a = 36$ kJ mol^{-1} and $\tau_0 = 3 \times 10^{-14}$ s for the hydrated form. In both phases, protons diffuse faster in the hydrated form than in the anhydrous form. The proton conductivities estimated from the NMR results for the anhydrous form agree with the macroscopic values in literature.

DOI: 10.1103/PhysRevB.74.134303 PACS number(s): 66.30.Hs, 76.60.−k

I. INTRODUCTION

Research and development of fuel cells are actively performed because of their high efficiencies in electrical power generation and low pollution levels. Electrolyte materials working in the temperature range between 373 and 573 K are one of the keys to open a new generation in fuel cells, because the operating temperature of polymer electrolyte membrane fuel cells is limited to lower than 373 K by the necessity of humid atmospheres. Haile *et al.* demonstrated that water-soluble inorganic solid acid salts such as $CsHSO_4$ and CsH_2PO_4 are used successfully in H_2/O_2 and direct methanol fuel cells above 373 K.[1,2]

It is well known that a high proton conductivity is observed in a high-temperature phase of solid acid salts such as $MHXO_4$ and $M_3H(XO_4)_2$ (M=Cs, NH_4, Rb; X=S, Se) families.[3–6] In these compounds, tetrahedral XO_4 anions form hydrogen bond networks, and protons diffuse through the networks very rapidly in the superprotonic phase. Previously, we have studied proton dynamics in $CsHSO_4$ and $Rb_3H(SO_4)_2$ by means of ^{1}H solid-state NMR,[7–10] which is suitable to study the dynamics at atomic levels. We concluded that a motion breaking the hydrogen bonds is rate determining in proton diffusion. The microscopic motion studied by NMR well explained the macroscopic proton conductivity.

The superprotonic phase was also observed in pentacesium trihydrogen tetrasulfate (or tetraselenate) hydrate, $Cs_5H_3(XO_4)_4 \cdot xH_2O$ (X=S, Se).[11,12] $Cs_5H_3(SO_4)_4 \cdot xH_2O$ exhibits a phase transition to the superprotonic phase at about 410 K.[12,13] A number of works have been performed on a glasslike state in this compound at low temperatures, in which disordered hydrogen bond networks were discussed.[14–20] The hydrogen bond network is dynamically disordered in the superprotonic phase.[12] There is an orientational disorder of SO_4 tetrahedra as well as a positional and orientational disorder of hydrogen bonds. A characteristic feature of $Cs_5H_3(SO_4)_4 \cdot xH_2O$ is that the disordered hydrogen bond network exists even in the room-temperature phase.[12] The disorder is dynamic at room temperature,[12] and it becomes static on cooling, forming a dipolar glasslike state.[14–16] Nonstoichiometry of the water content in $Cs_5H_3(SO_4)_4 \cdot xH_2O$ ($x \approx 0.5$) was thought to stabilize the disordered phase.[21,22] It has been reported that the crystalline water influences the stability of the dynamically disordered hydrogen bond network phase and the protonic conductivity in the family compounds such as $Cs_5H_3(SeO_4)_4 \cdot xH_2O$ and $K_5H_3(SO_4)_4 \cdot xH_2O$.[21,22] The water-stoichiometric compounds (x=1) were thought to form a phase with an ordered hydrogen bond network at low temperatures.[21,22] However, few works determined the water content experimentally. Consequently, the influence of the crystalline water has not been revealed yet.

In the present work, we have studied proton dynamics in $Cs_5H_3(SO_4)_4 \cdot xH_2O$ microscopically by means of ^{1}H solid-state NMR. NMR has the advantage of observing both acid protons and water directly. Water protons can be detected separately from acidic protons by using high-resolution solid-state NMR techniques, if present. We have checked the water content carefully. We have measured and analyzed ^{1}H spectral line shapes and spin-lattice relaxation times. We also present ^{1}H high-resolution solid-state NMR spectra, which can distinguish different proton species. We discuss the mechanism of proton transport as well as the role of crystalline water in the proton transport. The conclusions obtained in the present work are much different from the previous works, especially as for the influence of the crystalline water. An anhydrous state is confirmed in this work for the first time.

II. EXPERIMENTAL

A. Materials

Cesium sulfate (Cs_2SO_4, 99.9%) and sulfuric acid (H_2SO_4, 95%) were obtained from the Junsei Chemical Co., Ltd. (Tokyo). $Cs_5H_3(SO_4)_4 \cdot xH_2O$ crystals were grown by slow evaporation of the aqueous solution containing stoichiometric amounts of Cs_2SO_4 and H_2SO_4. The crystalline powder obtained was dried in a vacuum desiccator under a reduced pressure, which was an as-grown sample.

B. X-ray powder diffraction and thermal analyses

The x-ray powder diffraction pattern was measured by a Rigaku MiniFlex diffractometer with Cu Kα radiation at room temperature.

The thermogravimetric and differential thermal analyses (TG-DTA) were performed by Rigaku Thermo Plus TG 8120 under N_2 flow. The temperature was changed in the range of 298–573 K. The differential scanning calorimetry (DSC) was measured with Rigaku Thermo Plus DSC 8230 in a static N_2 atmosphere. The sample temperature was changed repeatedly in the range of 153–573 K. The temperature of the heat anomaly was defined as the start of the peak, not the peak position.

C. NMR measurements

The ^{1}H magic-angle-spinning (MAS) NMR spectra were traced at room temperature using a Bruker MSL400 spectrometer at Larmor frequency of 400.13 MHz. A Bruker MAS probehead was used with a zirconia rotor of 4.0-mm outer diameter. The ordinary single pulse sequence was used with a $\pi/4$ pulse and a recycle delay of 50 s. The frequency scale of the spectrum was expressed with respect to neat tetramethylsilane (TMS) by adjusting the signal of adamantane spinning at 8.0 kHz to 1.87 ppm.[9]

The ^{1}H static NMR spectra were measured with a Bruker ASX200 spectrometer at 200.13 MHz in the range of 170–500 K. A Bruker probehead with a solenoid coil was used. The solid echo pulse sequence ($90°_x$-τ_1-$90°_y$-τ_2-echo) was used to trace the spectra and the latter half of the echo signal was Fourier transformed. The τ_1 and τ_2 values were set at 8.0 μs. The frequency scale of the spectrum was expressed with respect to neat TMS by adjusting the signal of pure H_2O to 4.877 ppm.[23]

The ^{1}H T_1 values were measured with a Bruker ASX200 spectrometer at 200.13 MHz in the range of 230–500 K. The pulse sequences used were the inversion recovery and the progressive saturation recovery followed by the solid echo pulse sequence, which were $180°$-τ-$90°_x$-τ_1-$90°_y$-τ_2-echo and $(90°$-$\tau_3)_n$-τ-$90°_x$-τ_1-$90°_y$-τ_2-echo, respectively. The values of τ_1, τ_2, and τ_3 were 8.0, 8.0, and 30 μs, respectively. The T_1 values were also measured by a Bruker Minispec mq20 spectrometer at 19.65 MHz in the range of 230–480 K to clarify the frequency dependence of T_1. The inversion recovery ($180°$-τ-$90°$) and the saturation recovery ($90°$-τ-$90°$) pulse sequences were used, where τ denoted the variable delay time.

The as-grown sample and a sample dried *in vacuo* at 373 K were sealed in glass tubes with helium gas for measurements of static NMR spectra and spin-lattice relaxation times (T_1).

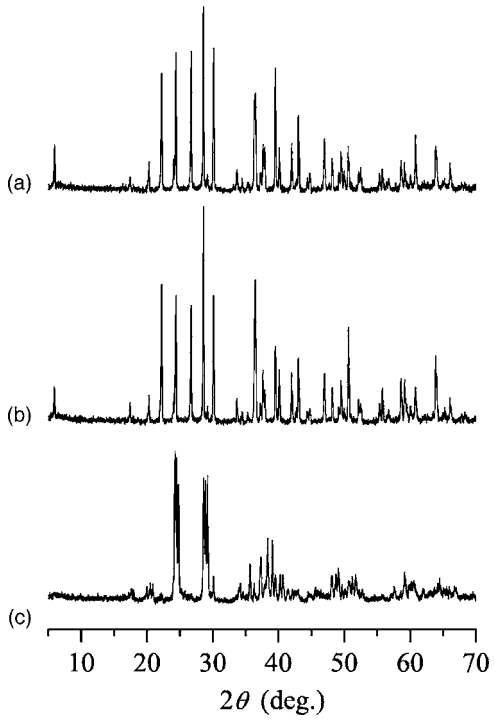

FIG. 1. X-ray powder diffraction patterns of (a) the as-grown sample and the samples heated at (b) 333 K and (c) 423 K in air atmosphere before the measurements.

III. RESULTS AND DISCUSSION

A. X-ray powder diffraction

Figure 1 shows x-ray powder diffraction patterns of samples after different pretreatments. The pattern of the as-grown sample [Fig. 1(a)] agrees well with that of the hexagonal phase of $Cs_5H_3(SO_4)_4 \cdot xH_2O$.[12] Heat treatment at 333 K causes negligible changes in the pattern, as shown in Fig. 1(b). The sample heated at 423 K shows a different pattern at room temperature, as shown in Fig. 1(c). The sample heated at 473 K shows the similar pattern at room temperature. This pattern is kept for 1 day in air atmosphere at room temperature. The original pattern is recovered after 3 days.

B. Thermal analyses

Figure 2 shows TG-DTA results for the as-grown sample. The mass gradually decreases with increase in temperature from room temperature to about 420 K. The mass loss in Fig. 2 is 0.73%, corresponding to 0.43 H_2O. The mass loss depends slightly on the drying conditions in the vacuum desiccator. An endothermic peak starting at 417 K is observed, which is ascribed to a superprotonic phase transition. A mass loss is also observed above 510 K, which is decomposition. An endothermic heat anomaly is observed at 540 K, which might be melting.

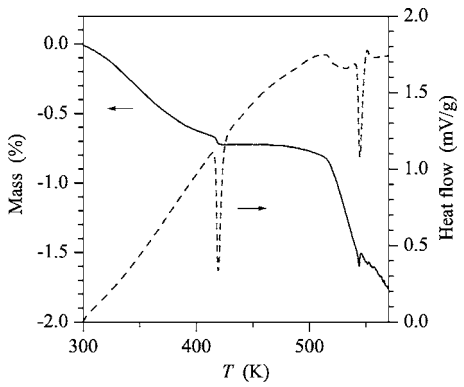

FIG. 2. TG-DTA curves for the as-grown sample, measured under N_2 flow. The temperature was changed from 298 K to 573 K with a rate of 5 K min^{-1}. The solid line indicates the mass of the sample, while the chain line indicates the DTA result. Negative heat flow is endothermic.

The phase relation is examined in detail by DSC, as shown in Fig. 3. The highest temperature is limited to lower than 500 K, to prevent from decomposition. The as-grown sample shows no heat anomaly on cooling down to 153 K. Heating the as-grown sample at 373 K loses the hydrated water, resulting in an anhydrous sample. The anhydrous sample shows a small heat anomaly at about 227 K on both cooling and heating (−2.20 J g^{-1} on heating). The sample transforms to a high-temperature phase (phase HT) at 420 K (−28.4 J g^{-1}). With decrease in temperature, an exothermic heat anomaly is observed at 371 K (27.4 J g^{-1}), and no peak is observed around 230 K. This sample shows a small endothermic peak at 399 K (−2.93 J g^{-1}) in addition to the superprotonic phase transition at 420 K (−25.1 J g^{-1}). The similar DSC curves are reproducibly observed when the sample temperature is cycled in the same range.

Further increase in temperature shows a small endothermic heat anomaly at 533 K (−0.845 J g^{-1}) and a melting peak at 540 K (−25 J g^{-1}). The melting is accompanied by decomposition.

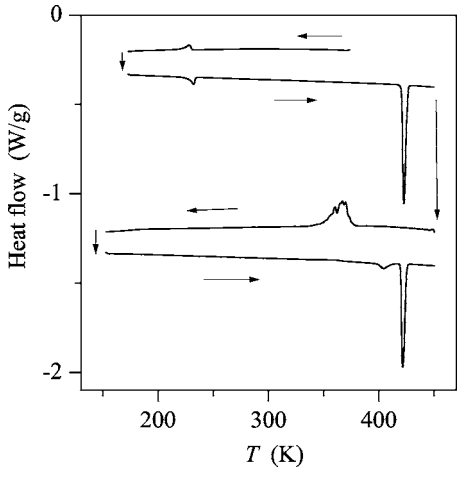

FIG. 3. DSC curves for the as-grown sample, measured under static N_2 gas. The temperature was changed from 373 K to 173 K, to 450 K, to 153 K, and to 450 K with a rate of 5 K min^{-1}. Negative heat flow is endothermic. The arrows indicate the order of the experiment.

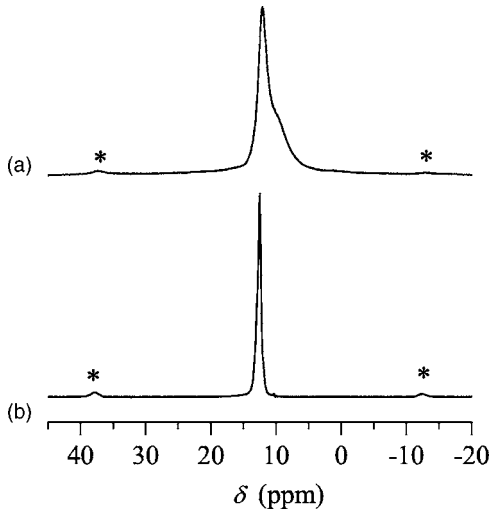

FIG. 4. ^{1}H MAS NMR spectra for (a) the as-grown sample and (b) a sample dried in vacuo at 373 K, measured at 400.13 MHz and at room temperature. The spinning rate of the sample was set at 10 kHz. The peaks marked by * are spinning sidebands.

C. ^{1}H MAS NMR spectra

Figure 4 shows ^{1}H MAS NMR spectra observed at room temperature. The spectrum of the as-grown sample shows a peak at 10.9 ppm with a shoulder centered at 9.7 ppm. The dried sample has only one peak at 11.2 ppm, which is ascribed to acidic protons. This means that all the proton sites are equivalent. No peak is observed around 5 ppm even in the as-grown sample, indicating that there is no physically adsorbed water and that the hydrated water is not in the form of H_2O. The signal at 10.9 ppm for the as-grown sample is ascribable to acidic protons. This signal has a little broader linewidth than the 11.2-ppm signal in the dried sample. On the other hand, the signal at 9.7 ppm is assigned to H_3O^+, being based on its chemical shift. This fact means that the crystalline water is present in the form of H_3O^+. The dried sample loses the crystalline water, and thus it is anhydrous. Separate observation of the acidic protons and H_3O^+ indicates that proton exchange between them is slower than the separation of the signal (1.2 ppm=480 Hz) at room temperature.

Eckert *et al.* presented the following relationship between the ^{1}H chemical shift and the hydrogen-bond strength:[24]

$$\delta_{\mathrm{iso}}(\mathrm{ppm}) = 79.05 - 255d(\mathrm{O\text{-}H\cdots O})(\mathrm{nm}), \qquad (1)$$

where δ_{iso} is an isotropic chemical shift and d(O-H···O) is the O-H···O distance. The ^{1}H chemical shift increases with the hydrogen-bond strength. Equation (1) predicts the O-H···O distances of 0.2673 and 0.2661 nm for the 10.9-ppm and 11.2-ppm signals, respectively. The crystal structure study reports the O-H···O distances of 0.268, 0.289, and 0.303 nm for the hydrated compound.[12] It also reports the O-H···O distances between H_2O and SO_4 (0.260 nm), which is rather short.[12] The dried sample shows

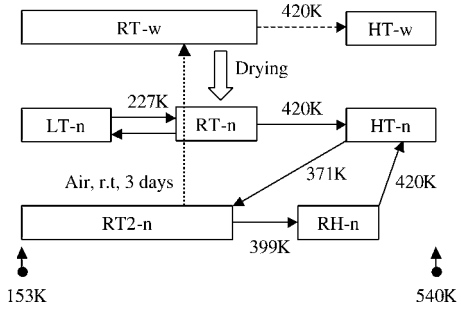

FIG. 5. Phase relations. RT is a room-temperature phase, HT is a high-temperature phase, LT is a low-temperature phase, and RH is an intermediate phase between phases RT and HT. The characters, w and n, after the phase name indicate "water" (hydrated) and "no water" (anhydrous), respectively. The solid arrows are the results of thermal analyses, while the chain and the dotted arrows are the results of NMR and x-ray powder diffraction, respectively.

a very sharp line, demonstrating a homogeneous strength of the hydrogen bonds. The crystal structure of the anhydrous compound is not known, although it is similar to the hydrated one. The observed signal positions are comparable to those for $CsHSO_4$ (11.2 ppm for phases II).[9]

The acidic protons show only one signal in both the hydrated and the dried samples, although the crystal structure study indicates the presence of several inequivalent hydrogen bonds. This observation strongly supports the presence of the dynamically disordered hydrogen bond network.

D. Phase relations

Phase relations in $Cs_5H_3(SO_4)_4 \cdot xH_2O$ are illustrated in Fig. 5, based on the results of thermal analyses as well as x-ray powder diffraction and ^{1}H MAS NMR. The as-grown sample is a room-temperature phase of the hydrated state $Cs_5H_3(SO_4)_4 \cdot 0.5H_2O$ (phase RT-w). It loses its hydrated water easily on heating, resulting in a room-temperature phase of the anhydrous state $Cs_5H_3(SO_4)_4$ (phase RT-n). Phases RT-w and RT-n have similar structures. Phase RT-n transforms to a low-temperature phase (phase LT-n) at 227 K and to a high-temperature phase (phase HT-n) at 420 K. The phase transition between phases RT-n and LT-n is quite reversible. Phase HT-n transforms to another room-temperature phase of the anhydrous state (phase RT2-n), whose structure is much different from that of phase RT-n, on cooling. Phase RT2-n transforms to phase HT-n through an intermediate phase (phase RH-n). Phase HT-n begins to decompose above 520 K and melts at 540 K. Phases RT-w, LT-n, and RT2-n are stable down to 153 K. Phase RT2-n transforms slowly to either phase RT-w or RT-n in ambient atmosphere at room temperature, probably to phase RT-w due to absorption of atmospheric moisture. Phase RT-w transforms to a high-temperature phase of the hydrated state (phase HT-w) at 420 K when the sample is sealed, which is confirmed by ^{1}H T_1 results described below.

E. ^{1}H static NMR spectra

The ^{1}H static NMR spectra were measured for sealed samples in the range of 170–500 K. The thermal history of the sample was taken into consideration in the measurements. The results presented below are concerned with phases LT, RT, and HT, and not with phases RT2-n and RH-n.

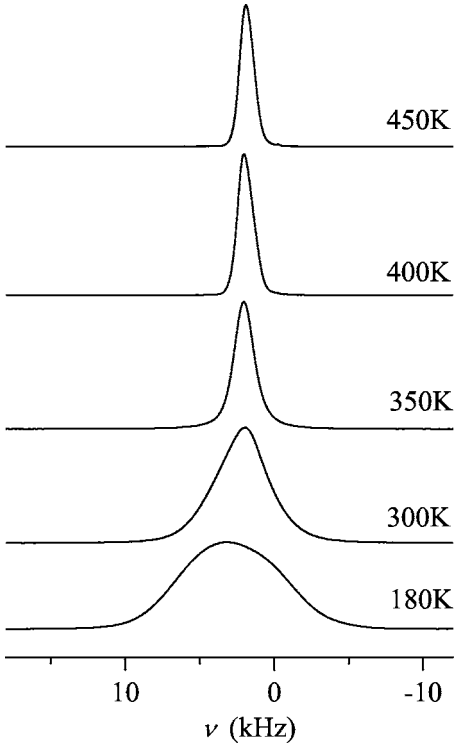

FIG. 6. ^{1}H static NMR spectra of the as-grown sample, measured at 200.13 MHz by raising the temperature.

Figure 6 shows some typical ^{1}H static NMR spectra of the as-grown sample, measured by raising the temperature. Only one signal is observed, and motional narrowing takes place. Temperature dependence of the linewidth is shown in Fig. 7. The linewidth decreases gradually up to 260 K, and then the decrease becomes rapid. The narrowing completes at 380 K.

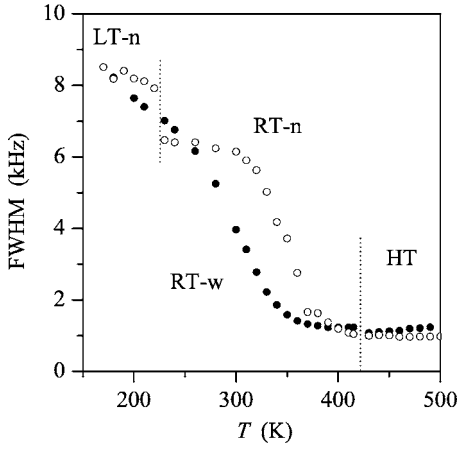

FIG. 7. Temperature dependence of the full width at half maximum (FWHM) in ^{1}H static NMR spectra. Solid and open circles are the values measured with increasing temperature for the as-grown sample and the dried sample, respectively. The vertical dotted lines indicate the temperatures of the phase transition.

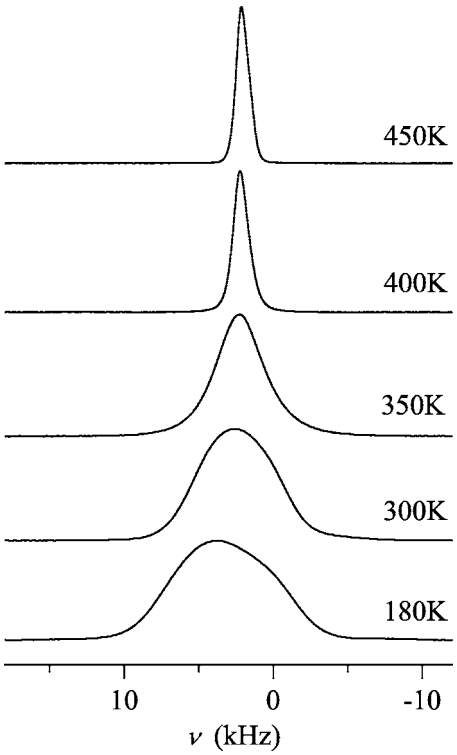

FIG. 8. ^{1}H static NMR spectra of the dried sample, measured at 200.13 MHz by raising the temperature.

No discontinuous change is observed at the phase transition of 420 K.

Figure 8 shows ^{1}H static NMR spectra of a sample dried at 373 K in vacuo. Similarly to the as-grown sample, only one signal is observed, and motional narrowing takes place, although the temperature range of the narrowing is higher than that for the as-grown sample. Figure 7 shows temperature dependence of the linewidth. There is a phase transition at 227 K. Below this temperature the linewidth is about 8.2 kHz, and at 230 K the linewidth discontinuously decreases to 6.5 kHz. Above 300 K the linewidth decreases rapidly, and the narrowing completes at about 400 K. No discontinuous change is observed at the phase transition of 420 K.

A very broad component appears below 260 K only for the as-grown sample, as shown in Fig. 9. This component comes from H_2O, because the dried sample does not have such a component. The ^{1}H MAS NMR results demonstrate that the crystalline water is present in the form of H_3O^+. The reorientation of H_3O^+ is gradually frozen with decrease in temperature below 260 K.

The component ascribed to the acidic protons show an asymmetric line shape at low temperatures for both the as-grown sample and the dried sample. This asymmetry might be caused by chemical shift anisotropy. The similar asymmetric line shapes have also been observed at low temperatures in $CsHSO_4$ and $Rb_3H(SO_4)_2$.[7,10]

The second moment is useful to identify modes of motions. Figure 10 shows temperature dependence of the second moment. The very broad component at the lower temperatures is omitted in the estimation.

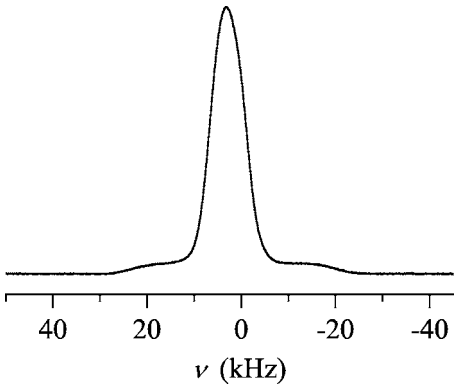

FIG. 9. ^{1}H static NMR spectra of the as-grown sample, measured at 200.13 MHz and at 180 K.

The second moments in a rigid state can be calculated from the crystal structure. In $Cs_5H_3(SO_4)_4 \cdot xH_2O$, ^{1}H and ^{133}Cs spins are taken into account, while S and O can be neglected. The ^{1}H linewidth has usually its origin in the dipolar interactions with ^{1}H and ^{133}Cs. The second moments for powder samples are given by[25,26]

$$M_2 = M_{\mathrm{HH}} + M_{\mathrm{HCs}}, \tag{2}$$

$$M_{\mathrm{HH}} = \frac{3}{5}\frac{\gamma_{\mathrm{H}}^4 \hbar^2}{4\pi^2} I_{\mathrm{H}}(I_{\mathrm{H}}+1)\sum_i \frac{1}{r_i^6}, \tag{3}$$

$$M_{\mathrm{HCs}} = \frac{4}{15}\frac{\gamma_{\mathrm{H}}^2 \gamma_{\mathrm{Cs}}^2 \hbar^2}{4\pi^2} I_{\mathrm{Cs}}(I_{\mathrm{Cs}}+1)\sum_j \frac{1}{r_j^6}, \tag{4}$$

where M_{HH} and M_{HCs} are the second moments due to ^{1}H-^{1}H and ^{1}H-^{133}Cs dipole-dipole interactions, respectively, in Hz^2 units, γ_{H} and γ_{Cs} are gyromagnetic ratios of ^{1}H and ^{133}Cs spins, respectively, $\hbar$ is Planck constant divided by

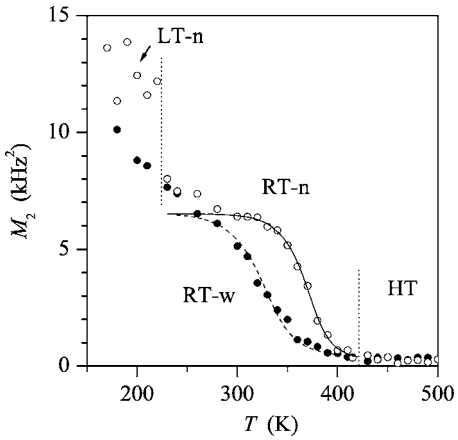

FIG. 10. Temperature dependence of the second moment (M_2) in ^{1}H static NMR spectra. Solid and open circles are the values measured with increasing temperature for the as-grown sample and the dried sample, respectively. The solid line and the chain line are the simulated results. The vertical dotted lines indicate the temperatures of the phase transition. The very broad component in the as-grown sample was neglected.

2π, r_i and r_j are distances between ^{1}H spins and between ^{1}H and ^{133}Cs spins, respectively, and I_H and I_{Cs} are nuclear spin quantum numbers of ^{1}H and ^{133}Cs spins, which are 1/2 and 7/2, respectively.

For an anhydrous compound, the structure is assumed to be the one constructed by simply removing water molecules from the crystal structure of phase RT-w.[12] In a rigid state, M_2=8.0 kHz^2, in which M_{HH}=4.7 kHz^2 and M_{HCs} =3.3 kHz^2. If all the SO_4 tetrahedra reorient fast enough, M_2=5.2 kHz^2, in which M_{HH}=3.1 kHz^2 and M_{HCs} =2.1 kHz^2.

The observed M_2 value at 230 K is 8 kHz^2 for the anhydrous compound, which might correspond to the rigid state. It decreases gradually to 6.5 kHz^2 at 300 K. This value is larger than the calculated value for the state of fast isotropic SO_4 reorientation. A part of SO_4 tetrahedra reorients isotropically, or SO_4 tetrahedra undergo an anisotropic motion. The crystal structure study demonstrates that a part of SO_4 tetrahedra has disordered orientations.[12] The observed M_2 value of the low-temperature phase (phase LT-n) below 227 K is about 12.5 kHz^2. The hydrogen bond network might become ordered in phase LT-n.

For a hydrated compound, H_2O is combined with H^+, forming H_3O^+. First, H_3O^+ is assumed to reorient isotropically fast enough. If the SO_4 tetrahedra are in a rigid state, M_2=8.7 kHz^2, in which M_{HH}=5.53 kHz^2 and M_{HCs} =3.13 kHz^2. If all the SO_4 tetrahedra reorient isotropically fast enough, M_2=6.8 kHz^2, in which M_{HH}=4.45 kHz^2 and M_{HCs}=2.35 kHz^2.

The observed M_2 value for the hydrated sample decreases gradually, and thus it is difficult to find a plateau. The decrease in M_2 below 260 K comes from H_3O^+ reorientation. Although the signal of H_3O^+ is removed in the M_2 estimation below 260 K, the other acidic protons suffer from the dipolar interaction with H_3O^+. Although the calculated value of 6.8 kHz^2 is near the inflection point (5 kHz^2 at 300 K), it is unlikely that all the SO_4 tetrahedra reorient isotropically fast enough, because no translational diffusion of protons takes place at this temperature. It is likely that a part of SO_4 tetrahedra undergoes an anisotropic motion from the crystal structure study demonstrating that a part of SO_4 tetrahedra have disordered orientations.[12]

The second moment decreases rapidly with temperature above 330 K and 280 K for the dried sample and the as-grown sample, respectively, and reaches about 0.5 kHz^2 at about 400 K. This small value indicates that protons undergo translational diffusion. The temperature dependence of the second moment is analyzed by the following equation:[25]

$$M_2(T) = M_{T2} + (M_{T1} - M_{T2})\frac{2}{\pi}\tan^{-1}[2\pi\beta(T)\tau_c(T)], \quad (5)$$

where $M_2(T)$, M_{T1}, and M_{T2} are the second moments at a given temperature (T), at lower temperatures and at higher temperatures, respectively. The $\beta(T)$ value corresponds to a linewidth; $\beta=(M_2)^{1/2}$ when the line shape is Gaussian. The $\tau_c(T)$ value is a correlation time. In the present case, τ_c $=0.5\tau_H$, where τ_H denotes a mean residence time of H, because the mutual dipolar interaction between ^{1}H spins is dominant. The τ_H value is a function of temperature, and it is assumed to obey Arrhenius relation as

$$\tau_H(T) = \tau_0 \exp\left(\frac{E_a}{RT}\right), \quad (6)$$

where τ_0 is a mean residence time at the infinite temperature or the inverse of a frequency factor, E_a is an activation energy, and R is the gas constant.

The second moment values of phase RT in Fig. 10 are fitted to Eq. (5). The obtained parameters are E_a =49 kJ mol^{-1}, $\tau_0=1.8\times10^{-11}$ s, M_{T1}=6.5 kHz^2, and M_{T2} =0.2 kHz^2 for the dried sample and E_a=31 kJ mol^{-1}, τ_0 $=2.2\times10^{-9}$ s, M_{T1}=6.5 kHz^2, and M_{T2}=0.3 kHz^2 for the as-grown sample. The obtained values are only tentative for the as-grown sample, because the low-temperature value cannot clearly be defined.

The second moments in phase HT are 0.2 and 0.3 kHz^2 for the dried sample and the as-grown sample, respectively. Those values mean that protons diffuse as translational. No discontinuous change is observed at the phase transition temperature, because the motional narrowing completes below the transition temperature.

The as-grown sample contains two types of protons, the acidic proton and H_3O^+, as indicated by the ^{1}H MAS NMR spectra. The ^{1}H static NMR spectra do not show different line shapes for the two types of protons, except below 260 K. This indicates that all protons including those in H_3O^+ take part in proton diffusion at high temperatures. Proton exchange between the acidic proton and H_3O^+ takes place.

F. ^{1}H spin-lattice relaxation times

The relaxation curves are single exponential at both 200.13 and 19.65 MHz. Figures 11 and 12 show the T_1 values obtained for the as-grown sample and the dried sample, respectively. For the as-grown sample, the T_1 values decrease with increase in temperature below 300 K, and then they increase. The T_1 values change discontinuously at 420 K, indicating a presence of the transition from phases RT-w to HT-w. In phase HT-w, the T_1 values increase slightly with temperature.

For the dried sample, the temperature dependence is similar to that for the as-grown sample. In phase RT-n the T_1 values decrease with increase in temperature below 300 K, and then they increase. The T_1 values begin to decrease just below the transition temperature from phases RT-n to HT-n. They change discontinuously at the transition. In phase HT-n, the T_1 values decrease slightly with temperature.

Temperature and frequency dependences of the T_1 values are analyzed theoretically. Fluctuation of dipole-dipole interaction is the most dominant relaxation mechanism in the present system. As described above, ^{1}H and ^{133}Cs spins should be taken into account in $Cs_5H_3(SO_4)_4\cdot xH_2O$, while S and O can be neglected. Consequently, the ^{1}H spin-lattice relaxation is caused by fluctuation of the dipole-dipole interactions between ^{1}H spins and between ^{1}H and ^{133}Cs spins.

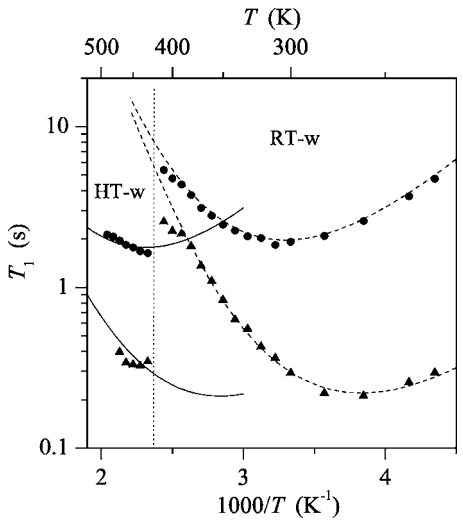

FIG. 11. Temperature and frequency dependences of ^{1}H T_1 of the as-grown sample. Circles and triangles indicate the results measured with increasing temperature at 200.13 and 19.65 MHz, respectively. The chain lines and the solid lines are the simulated curves for phases RT-w and HT-w, respectively. The vertical dotted line indicates the temperature of the phase transition.

According to the theory of Bloembergen, Purcell, and Pound (BPP),[25,27] the dipolar contribution to the spin-lattice relaxation is written as

$$T_{1d}^{-1} = \frac{8\pi^2}{3}\Delta M_{HH}\left[\frac{\tau_{HH}}{1+(\omega_H\tau_{HH})^2} + \frac{4\tau_{HH}}{1+4(\omega_H\tau_{HH})^2}\right] + 4\pi^2\Delta M_{HCs}\left[\frac{0.5\tau_{HCs}}{1+\{(\omega_H-\omega_{Cs})\tau_{HCs}\}^2} + \frac{1.5\tau_{HCs}}{1+(\omega_H\tau_{HCs})^2} + \frac{3\tau_{HCs}}{1+\{(\omega_H+\omega_{Cs})\tau_{HCs}\}^2}\right], \quad (7)$$

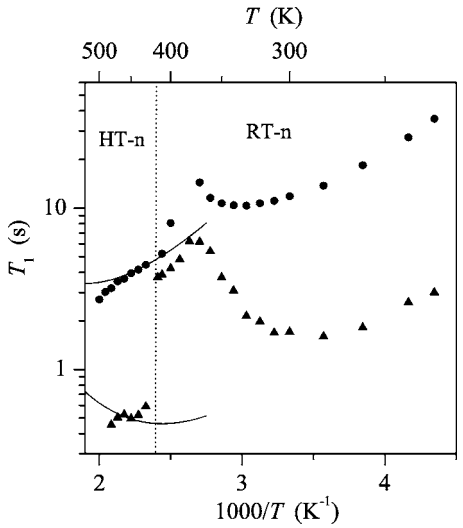

FIG. 12. Temperature and frequency dependences of ^{1}H T_1 of the dried sample. Circles and triangles indicate the results measured with increasing temperature at 200.13 and 19.65 MHz, respectively. The solid lines are the simulated curves for phase HT-n. The vertical dotted line indicates the temperature of the phase transition.

where ω_H and ω_{Cs} are angular resonance frequencies of ^{1}H and ^{133}Cs, respectively. The values of ΔM_{HH} and ΔM_{HCs} are the second moments contributing to the relaxation due to ^{1}H-^{1}H and ^{1}H-^{133}Cs dipole-dipole interactions, respectively, in Hz^2 units. The values of τ_{HH} and τ_{HCs} are correlation times between ^{1}H spins and between ^{1}H and ^{133}Cs. Assuming that only H is mobile, the correlation times between ^{1}H spin and the other spins are as follows: $\tau_{HCs}=\tau_H$, where τ_H is a mean residence time of H. On the other hand, $\tau_{HH}=0.5\tau_H$ if a proton and its surrounding protons are both mobile.

Another relaxation mechanism to be considered is fluctuation of ^{1}H anisotropic chemical shift. The anisotropy amounts to about 25 ppm (5.0 kHz at Larmor frequency of 200.13 MHz) in KH_2PO_4.[28] Fluctuation of anisotropic chemical shift contributes to the relaxation as follows:[25]

$$\frac{1}{T_{1c}} = \frac{3}{10}\omega_H^2(\Delta C_{anis})^2\frac{\tau_H}{1+\omega_H^2\tau_H^2}, \quad (8)$$

where ΔC_{anis} is the square root of the difference between the $\delta_{anis}^2(1+\eta_C^2/3)$ values at low and high temperatures. Three principal components of a chemical shift tensor (δ_{11}, δ_{22}, and δ_{33}) are defined as $|\delta_{33}-\delta_{iso}| \geqslant |\delta_{11}-\delta_{iso}| \geqslant |\delta_{22}-\delta_{iso}|$. The δ_{iso} value is an isotropic chemical shift, which is

$$\delta_{iso} = \frac{1}{3}(\delta_{11}+\delta_{22}+\delta_{33}). \quad (9)$$

The η_C value is an asymmetry factor and defined as

$$\eta_C = \frac{\delta_{22}-\delta_{11}}{\delta_{33}-\delta_{iso}} \quad (0 \leqslant \eta_C \leqslant 1). \quad (10)$$

The δ_{anis} value is the magnitude of chemical shift anisotropy and defined as

$$\delta_{anis} = \delta_{33} - \delta_{iso}. \quad (11)$$

The contribution of this mechanism increases with Larmor frequency.

Both the dipole-dipole interaction and the anisotropic chemical shift interaction contribute to the relaxation

$$\frac{1}{T_1} = \frac{1}{T_{1d}} + \frac{1}{T_{1c}}. \quad (12)$$

We have attempted to fit the temperature and frequency dependences of ^{1}H T_1 to Eq. (12), but it failed. Consequently, the BPP-type equations are modified by assuming a log-normal distribution of mean residence times, as performed in the previous works.[29,30] The relaxation time is expressed as

$$\frac{1}{T_1} = \int F(S)\left(\frac{1}{T_{1d}} + \frac{1}{T_{1c}}\right)dS. \quad (13)$$

$F(S)$ is a distribution function

$$F(S) = \frac{1}{\beta_1\sqrt{\pi}}\exp\left(-\frac{S^2}{\beta_1^2}\right), \quad (14)$$

$$S = \ln\frac{\tau_H}{\tau_{mH}}, \quad (15)$$

$$\beta_1^2 = \beta_0^2 + \left(\frac{\beta_Q}{RT}\right)^2, \tag{16}$$

$$\tau_{mH} = \tau_0 \exp\left(\frac{E_a}{RT}\right). \tag{17}$$

The symbols of β_0 and β_Q are parameters defining the magnitude of the distribution. They relate to the distributions of the preexponential factor and the activation energy centered by τ_0 and E_a, respectively. The symbol of τ_{mH} is the central value of the mean residence time at T. We have attempted to fit the temperature and frequency dependences of ^{1}H T_1 to Eq. (13).

In phase RT-w of the as-grown sample, the H_3O^+ reorientation causes the relaxation. Dipolar interaction between ^{1}H spins in the same H_3O^+ group relaxes the ^{1}H spins dominantly. Consequently, other dipolar interactions are neglected. In other words, $\Delta M_{HCs}=0$. The δ_{anis} value is assumed to be 25 ppm by analogy with KH_2PO_4,[28] and the η_C is assumed to be zero. Protons in H_3O^+ is 3/8 of all protons. Therefore, $(\Delta C_{anis})^2=\delta_{anis}^2\times(3/8)$. Intra-$H_3O^+$ group interaction works, and thus $\tau_{HH}=\tau_H$. The fitting shown by chain lines in Fig. 11 results in the parameters $E_a=35$ kJ/mol, $\tau_0=3.5\times10^{-16}$ s, $\beta_Q=7.5$ kJ/mol, $\beta_0=1.5$, and $\Delta M_{HH}=35$ kHz^2.

In phase RT-n of the dried sample, temperature dependence of T_1 is similar to that in phase RT-w, although the T_1 minimum values are about five times longer. H_2O is not removed completely in the dried sample, and the residual H_3O^+ relaxes surrounding protons.

The precise crystal structure of phase HT is unknown. Therefore, the calculated second moments for phase RT is used instead. All the protons are mobile, and thus $\tau_{HH}=0.5\tau_H$. The ΔC_{anis} value is assumed to be 25 ppm. For the as-grown sample, the fitting shown by solid lines in Fig. 11 results in the parameters $E_a=36$ kJ/mol, $\tau_0=3.0\times10^{-14}$ s, $\beta_Q=8.0$ kJ/mol, $\beta_0=2.0$, $\Delta M_{HH}=5.53\times2.6$ kHz^2, and $\Delta M_{HCs}=3.13\times2.6$ kHz^2. The factor of 2.6 needs to be introduced to adjust the T_1 minimum values. For the dried sample, the fitting shown by solid lines in Fig. 12 results in the parameters $E_a=34$ kJ/mol, $\tau_0=3.0\times10^{-13}$ s, $\beta_Q=8.0$ kJ/mol, $\beta_0=2.0$, $\Delta M_{HH}=4.74\times1.15$ kHz^2, and $\Delta M_{HCs}=3.26\times1.15$ kHz^2. The factor of 1.15 is introduced to adjust the T_1 minimum values.

G. Proton dynamics and conductivity

In phase RT, the acidic protons undergo translational diffusion, where the SO_4 reorientation is considered to be rate determining. The ^{1}H mean residence time for this motion is plotted in Fig. 13. The parameters for the reorientation are $E_a=49$ kJ mol^{-1} and $\tau_0=1.8\times10^{-11}$ s for the anhydrous form and $E_a=31$ kJ mol^{-1} and $\tau_0=2.2\times10^{-9}$ s for the hydrated form. The latter is comparable with that in phase II of $CsHSO_4$ ($E_a=35$ kJ mol^{-1}, $\tau_0=3.0\times10^{-9}$ s).[7] Note that the τ_H value for phase II of $CsHSO_4$ is corrected by multiplication of 2 because $\tau_H=2\tau_c$. The anhydrous form shows a slower motion than the hydrated form. The crystalline water might assist the proton translational diffusion.

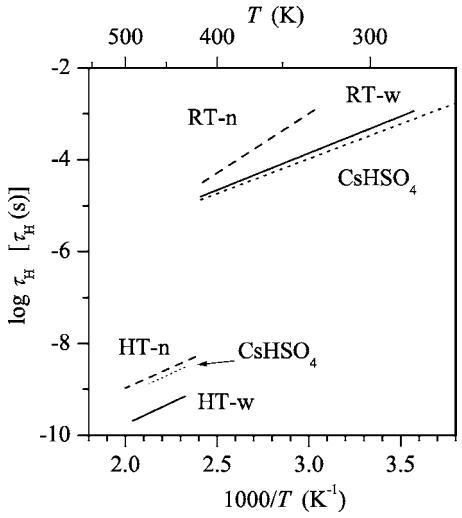

FIG. 13. ^{1}H mean residence times of the acidic protons. The solid lines correspond to the hydrated form, the chain lines to the anhydrous form of $Cs_5H_3(SO_4)_4\cdot xH_2O$ and the dotted lines to $CsHSO_4$ (Refs. 7 and 8).

In phase HT, which is superprotonic, the ^{1}H static NMR spectra indicate that the acidic protons undergo translational diffusion. From the analysis of ^{1}H T_1 results we have obtained parameters for the translational diffusion of the acidic protons: $E_a=34$ kJ mol^{-1} and $\tau_0=3\times10^{-13}$ s for the anhydrous form and $E_a=36$ kJ mol^{-1} and $\tau_0=3\times10^{-14}$ s for the hydrated form. Those parameters for the anhydrous form are comparable with those in the high-temperature phases (phase I) of $CsHSO_4$.[8] The hydrated form shows shorter mean residence times than the anhydrous form does. In phase HT also, the crystalline water enhances the proton translational diffusion.

Diffusion constants are related to the mean residence time of protons by the following equation:

$$D = \frac{L^2}{n\tau_H}, \tag{18}$$

where L is a jumping distance and n is the number of sites to which H can jump. The D value obeys Arrhenius relation as

$$D = D_0 \exp\left(-\frac{E_a}{RT}\right), \tag{19}$$

where D_0 is a constant independent of temperature.

The L value is estimated from the interatomic distances between H atoms in phase RT-w.[12] It is assumed to be 0.39 nm by averaging the distances. Because the crystal structure of phase HT is unknown, the L value is assumed to be 0.39 nm in phase HT as well. The n value is 6 for a powder sample. Using the τ_H value, thus, the D_0 values for the anhydrous form are 1.5×10^{-9} and 8.7×10^{-8} m^2 s^{-1} in phases RT-n and HT-n, respectively. On the other hand, the D_0 values for the hydrated form are 1.2×10^{-11} and 8.7×10^{-7} m^2 s^{-1} in phases RT-w and HT-w, respectively. The pulsed-field-gradient NMR study reported D values of 2.8×10^{-12} m^2 s^{-1} (414 K) to 4.4×10^{-12} m^2 s^{-1} (434 K).[13] These values are comparable with those for phase HT-n of

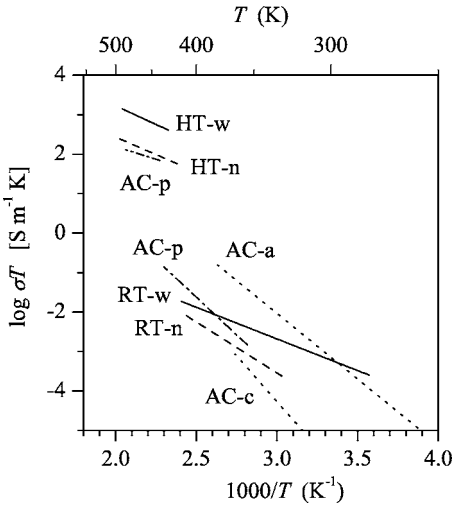

FIG. 14. Proton conductivities. HT-w, HT-n, RT-w, and RT-n are estimated from the NMR results of the corresponding phases. AC means the values obtained from the AC impedance method. AC-a and AC-c correspond to the *a* and *b* directions, respectively, in a single crystal,[21] while AC-p is a value for powder samples.[31,32]

the anhydrous form, which range from 5.1×10^{-12} m^2 s^{-1} (420 K) to 2.4×10^{-11} m^2 s^{-1} (500 K).

The electric conductivity is related to the proton diffusion constant by the following equation:

$$\sigma = Ne^2D/kT, \tag{20}$$

where N is the density of mobile protons, e is the proton charge, and k is Boltzmann constant. The σT value obeys Arrhenius relation as

$$\sigma T = A_0 \exp\left(-\frac{E_a}{RT}\right), \tag{21}$$

where A_0 is a constant independent of temperature.

The N value of the acidic protons is estimated as 5.98×10^{27} m^{-3} in phase RT from the crystal structure of the hydrated form,[12] and the same value is assumed for phase HT as well as for the anhydrous form. The A_0 values of the anhydrous form are 1.6×10^4 and 9.6×10^5 S m^{-1} K for phases RT-n and HT-n, respectively. On the other hand, the A_0 values of the hydrated form are 1.3×10^2 and 9.6×10^6 S m^{-1} K for phases RT-w and HT-w, respectively. The estimated conductivities for the superprotonic phase are shown in Fig. 14, together with some literature data. The conductivity of the anhydrous sample in the present work is comparable with those for a powder sample[31,32] and for the (001) direction in phase RT of a single crystal.[21] The hydrated form shows a higher conductivity in both phases.

IV. CONCLUSIONS

Phase relations and proton dynamics in $Cs_5H_3(SO_4)_4\cdot xH_2O$ have been studied by means of ^{1}H solid-state NMR as well as thermal analyses, and the following conclusions have been obtained:

(1) Complicated phase relations are revealed as illustrated in Fig. 5. We found the hydrated form $Cs_5H_3(SO_4)_4\cdot0.5H_2O$ and the anhydrous form $Cs_5H_3(SO_4)_4$. The superprotonic phase transition takes place at 420 K for both the hydrated and the anhydrous forms.

(2) The ^{1}H chemical shifts of the acidic protons are 10.9 and 11.2 ppm for the hydrated and the anhydrous forms, respectively. Those values are comparable with that in phase II of $CsHSO_4$, indicating the similar hydrogen bond strength. The observation of a single line for the acidic protons strongly supports the presence of the dynamically disordered hydrogen bond network. The hydrated sample shows a signal at 9.7 ppm additionally, which is ascribed to H_3O^+, not H_2O.

(3) In phase RT, translational diffusion of protons takes place in both compounds. The ^{1}H mean residence times are estimated from the second moment analysis. The parameters are E_a=49 kJ mol^{-1} and $\tau_0=1.8\times10^{-11}$ s for the anhydrous form and E_a=31 kJ mol^{-1} and $\tau_0=2.2\times10^{-9}$ s for the hydrated form. Protons diffuse faster in the hydrated form than in the anhydrous form.

(4) In phase HT also, protons diffuse as translational. From the analysis of ^{1}H T_1 results we have obtained parameters for the translational diffusion of protons: E_a=34 kJ mol^{-1} and $\tau_0=3\times10^{-13}$ s for the anhydrous form and E_a=36 kJ mol^{-1} and $\tau_0=3\times10^{-14}$ s for the hydrated form. In phase HT also, protons diffuse faster in the hydrated form than in the anhydrous form.

(5) The proton conductivities estimated from the NMR results for the anhydrous form agree with the macroscopic values in literature.

(6) The crystalline water affects the phase relation as well as the proton diffusion.

ACKNOWLEDGMENT

This work was financially supported by the New Energy and Industrial Technology Development Organization (NEDO).

*Present address: R&D Division, Energy Business Group, Core Component Business Unit, Sony Corporation, 1-1 Takakura Aza Shimosugishita, Hiwada-machi, Koriyama-shi, Fukushima 963-0531, Japan.

†Corresponding author. Electronic address: hayashi.s@aist.go.jp

[1] S. M. Haile, D. A. Boysen, C. R. I. Chisholm, and R. B. Merle, Nature (London) **410**, 910 (2001).

[2] D. A. Boysen, T. Uda, C. R. I. Chisholm, and S. M. Haile, Science **303**, 68 (2004).

[3] A. I. Baranov, L. A. Shuvalov, and N. M. Shchagina, JETP Lett. **36**, 459 (1982).

[4] A. Pawlowski, Cz. Pawlaczyk, and B. Hilzcer, Solid State Ionics **44**, 17 (1990).

[5] T. Norby, M. Friesel, and B. E. Mellander, Solid State Ionics **77**,

105 (1995).
[6] V. V. Sinitsyn, A. I. Baranov, E. G. Ponyatovsky, and L. A. Shuvalov, Solid State Ionics **77**, 118 (1995).
[7] M. Mizuno and S. Hayashi, Solid State Ionics **167**, 317 (2004).
[8] S. Hayashi and M. Mizuno, Solid State Ionics **171**, 289 (2004).
[9] S. Hayashi and M. Mizuno, Solid State Commun. **132**, 443 (2004).
[10] K. I. Suzuki and S. Hayashi, Phys. Rev. B **73**, 024305 (2006).
[11] B. V. Merinov, A. I. Baranov, L. A. Shuvalov, and N. M. Shchagina, Sov. Phys. Crystallogr. **36**, 321 (1991).
[12] B. V. Merinov, A. I. Baranov, L. A. Shuvalov, J. Schneider, and H. Schulz, Solid State Ionics **74**, 53 (1994).
[13] A. M. Fajdiga-Bulat, G. Lahajnar, J. Dolinšek, J. Slak, B. Ložar, B. Zalar, L. A. Shuvalov, and R. Blinc, Solid State Ionics **77**, 101 (1995).
[14] A. I. Baranov, O. A. Kabanov, B. V. Merinov, L. A. Shuvalov, and V. V. Dolbinia, Ferroelectrics **127**, 257 (1992).
[15] Y. Yuzyuk, V. Dmitriev, L. Rabkin, L. Burmistrova, L. Shuvalov, F. Smutný, P. Vanek, I. Gregora, and J. Petzelt, Solid State Ionics **77**, 122 (1995).
[16] Y. I. Yuzyuk, V. P. Dmitriev, L. M. Rabkin, F. Smutný, I. Gregora, V. V. Dolbinia, and L. A. Shuvalov, J. Phys.: Condens. Matter **8**, 3965 (1996).
[17] B. V. Merinov, R. Melzer, R. E. Lechner, D. J. Jones, and J. Rozière, Solid State Ionics **97**, 161 (1997).
[18] A. I. Baranov, E. D. Yakushkin, D. J. Jones, and J. Roziere, Solid State Ionics **125**, 99 (1999).
[19] S. G. Lushnikov, S. N. Gvasaliya, A. I. Fedoseev, V. H. Schmidt, G. F. Tuthill, and L. A. Shuvalov, Phys. Rev. Lett. **86**, 2838 (2001).
[20] S. N. Gvasaliya, A. I. Fedossev, S. G. Lushnikov, V. H. Schmidt, G. F. Tuthill, and L. A. Shuvalov, J. Phys.: Condens. Matter **13**, 3677 (2001).
[21] A. I. Baranov, V. V. Sinitsyn, V. Y. Vinnichenko, D. J. Jones, and B. Bonnet, Solid State Ionics **97**, 153 (1997).
[22] A. I. Baranov, Ferroelectrics **265**, 87 (2002).
[23] S. Hayashi, M. Yanagisawa, and K. Hayamizu, Anal. Sci. **7**, 955 (1991).
[24] H. Eckert, J. P. Yesinowski, L. A. Silver, and E. M. Stolper, J. Phys. Chem. **92**, 2055 (1988).
[25] A. Abragam, *The Principles of Nuclear Magnetism* (Oxford University Press, London, 1961).
[26] J. H. Van Vleck, Phys. Rev. **74**, 1168 (1948).
[27] N. Bloembergen, E. M. Purcell, and R. V. Pound, Phys. Rev. **73**, 679 (1948).
[28] J. T. Rasmussen, M. Hohwy, H. J. Jakobsen, and N. C. Nielsen, Chem. Phys. Lett. **314**, 239 (1999).
[29] E. R. Andrew, D. J. Bryant, and E. M. Cashell, Chem. Phys. Lett. **69**, 551 (1980).
[30] S. Hayashi and M. Mizuno, Solid State Ionics **176**, 745 (2005).
[31] G. V. Lavrova and V. G. Ponomareva, Inorg. Mater. **38**, 1172 (2002).
[32] G. V. Lavrova, V. G. Ponomareva, and E. B. Burgina, Solid State Ionics **176**, 767 (2005).